frontiers in Energy Research

ORIGINAL RESEARCH
published: 06 July 2021
doi: 10.3389/fenrg.2021.713510

Assessment for Voltage Violations considering Reactive Power Compensation Provided by Smart Inverters in Distribution Network

Jindi Hu[1], Weibin Yin[2], Chengjin Ye[1], Weidong Bao[3], Jiajia Wu[3] and Yi Ding[1]*

[1]College of Electrical Engineering, Zhejiang University, Hangzhou, China, [2]State Grid Jiaxing Power Supply Company, Jiaxing, China, [3]State Grid Yiwu Power Supply Company, Yiwu, China

Due to the high proportion of renewable energies, traditional voltage regulation methods such as on-load tap changers (OLTCs) and switching capacitors (SCs) are currently facing the challenge of providing fast, step-less, and low-cost reactive power to reduce the increasing risks of voltage violations in distribution networks (DNs). To meet such increasing demand for voltage regulation, smart inverters, including photovoltaics (PVs) and electric vehicle (EV) chargers, stand out as a feasible approach for reactive power compensation. This paper aims to assess the voltage violation risks in DNs considering the reactive power response of smart inverters. Firstly, reactive power compensation models of PVs and EV chargers are investigated and voltage deviation indexes of the regulation results are proposed. Moreover, kernel density estimation (KDE) and slice sampling are adopted to provide the PV output and EV charging demand samples. Then, the risk assessment is carried out with a voltage regulation model utilizing OLTCs, SCs, and available smart inverters. Numerical studies demonstrate that the reactive power support from smart inverters can significantly mitigate the voltage violation risks and reduce the switching and cost of OLTCs and capacitors in DNs.

Keywords: distribution network, reactive power compensation, risk assessment, electric vehicle charger, photovoltaic

OPEN ACCESS

Edited by:
Yang Li,
Northeast Electric Power University, China

Reviewed by:
Huaiyuan Wang,
Fuzhou University, China
Gengfeng Li,
Xi'an Jiaotong University, China
Yunfei Mu,
Tianjin University, China

****Correspondence:***
Chengjin Ye
yechenjing@zju.edu.cn

Specialty section:
This article was submitted to Smart Grids, a section of the journal Frontiers in Energy Research

Received: *23 May 2021*
Accepted: *21 June 2021*
Published: *06 July 2021*

Citation:
Hu J, Yin W, Ye C, Bao W, Wu J and Ding Y (2021) Assessment for Voltage Violations considering Reactive Power Compensation Provided by Smart Inverters in Distribution Network. Front. Energy Res. 9:713510. doi: 10.3389/fenrg.2021.713510

1 INTRODUCTION

The development of power electronics in distribution networks (DNs) brings prosperity for distributed photovoltaics (PVs), electric vehicle (EV) chargers, and other devices with AC-DC inverters. However, DNs are more prone to voltage violation problems nowadays because of the uncertainty of PV outputs and the load impact of EV charging (Kekatos et al., 2015). Traditional reactive power compensation facilities such as on-load tap changers (OLTCs) and switching capacitors (SCs) are only able to provide step-wise and high-delay reactive power at the feeder head, which limits the regulation effect (Kekatos et al., 2015), while the high cost of Distribution Static Synchronous Compensators (D-STATCOMs) restricts its application in DNs (Chen et al., 2018). Therefore, it is of vital importance to implement step-less compensation facilities at the feeder terminal.

Meanwhile, the two-way reactive power ability of smart inverters (i.e., PVs and EV chargers in this paper) enables these terminal end power electronics in DNs to participate in voltage regulation. There have already been some investigations to achieve reactive power delivery from smart inverters.

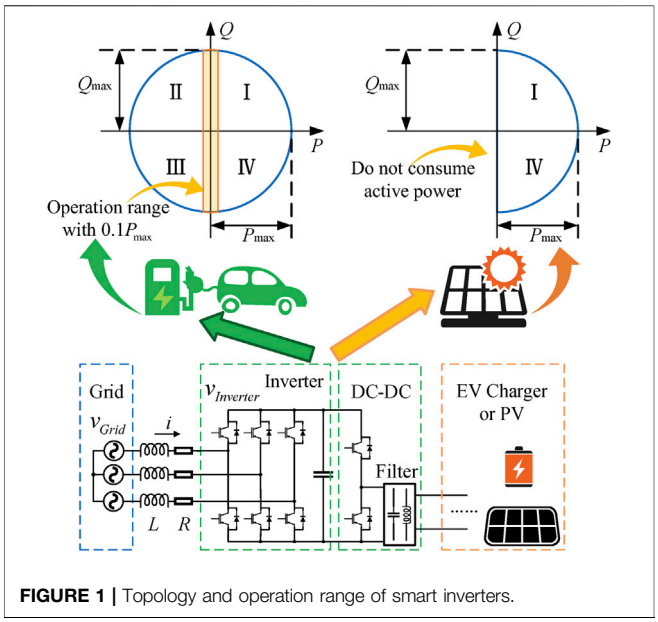

FIGURE 1 | Topology and operation range of smart inverters.

Sharma and Das (2020) and Feng et al. (2018) extend the reactive power exchange for PV inverters and help to balance the active and reactive power transmission of each phase. Buja et al. (2017) analyze and validate the reactive power compensation abilities of EV chargers theoretically and experimentally. Moreover, Varma and Siavashi (2018), Abeywardana et al. (2018), and Kesler et al. (2014) point out that the reactive power compensation process of PVs and EV chargers does not intervene in the active power delivery or cause damage to EV batteries, which expands the implementation of EV chargers to a large extent. To integrate these flexible power electronics, Varma and Siavashi (2018) present a novel smart inverter PV-STATCOM which controls PV inverters as a dynamic reactive power compensator. Furthermore, Singh et al. (2019) achieve voltage regulation through smart inverters of PVs and EV charging stations in the global as well as local domain. Smart inverters have been well investigated and developed to compensate reactive power (Ustun et al., 2020; Gush et al., 2021). Therefore, it is feasible to resort to smart inverters for accurate and fast voltage regulation in DNs.

The application of smart inverters to regulate voltage quality has been investigated. Zeraati et al. (2019) develop a distributed voltage regulation scheme to utilize the reactive power capability of PV inverters. Quirós-Tortós et al. (2016) and Singh et al. (2019) achieve reactive power control in DNs with the support of EV chargers and PVs. However, the voltage regulation techniques using smart inverters are still under research and need practical implementations. Therefore, it is essential to assess the voltage regulation effects of smart inverters to provide references for the market price of their reactive power compensation.

To assess the reliability of power systems, the Monte Carlo simulation is usually utilized to sample from the target distribution when considering the uncertainty of renewable energies or power demands (Zhou et al., 2016). It is applicable for common Monte Carlo methods, such as importance sampling (Tómasson and Sö) and acceptance-rejection sampling (Hu et al., 2017), to sample from a standard target distribution. However, the irregular PV outputs and EV loads require non-parametric estimation techniques to acquire their probability density functions (PDFs) and more universal sampling methods suitable for any non-standard PDF (Huang et al., 2020). Slice sampling is an advanced method of Markov Chain Monte Carlo (MCMC) simulation (Neal, 2003). It is feasible for PV outputs and EV loads owing to its ability to sample from irregular PDFs efficiently.

Based on the above analysis, this paper proposes a voltage violation assessment model considering the participation of smart inverters. Samples of PV outputs and EV loads are generated. The voltage violation assessment is carried out to evaluate the performance of smart inverters. The main contributions of this paper can be summarized as two-fold:

1. The quantitative compensation ability assessment of smart inverters is proposed with the available reactive power capacities under active power constraints. The optimization model for voltage regulation is established considering both traditional reactive power compensation facilities and smart inverters.
2. The voltage violation assessment under the uncertainty of PV outputs and EV behaviors is achieved based on the proposed voltage deviation indexes, non-parametric kernel density estimation (KDE), and slice sampling. The non-standard PDFs of PVs and EVs are fitted accurately by KDE. Besides, the automated step width selection for slice

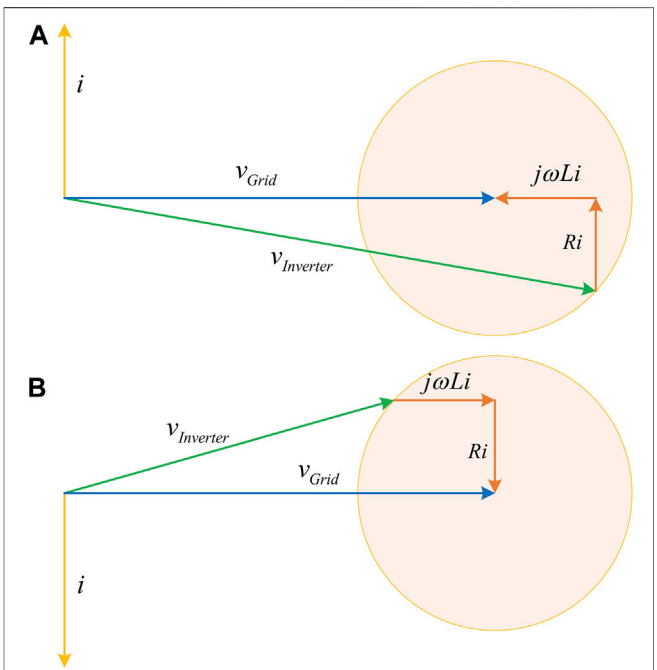

FIGURE 2 | Voltage vector diagrams of two typical operation modes **(A)** is the capacitive mode **(B)** is the inductive mode.

sampling is adopted to efficiently generate samples from the obtained PDFs. The results demonstrate that smart inverters have better voltage regulation effects and are able to reduce the operation cost of OLTCs and SCs.

The remaining of this paper is organized as follows. **Section 2** describes the basic models and voltage deviation indexes for voltage regulation. KDE and slice sampling are introduced in **Section 3**. **Section 4** illustrates the risk assessment process for voltage violations. Numerical studies are presented in **Section 5**. Finally, **Section 6** concludes this paper.

2 BASIC MODELS

2.1 Reactive Power Compensation Mechanism of Smart Inverters

The AC-DC inverters of EV chargers and PVs are composed of controllable power electronics with a three-phase six-pulse topology. The equivalent smart inverter models are depicted in **Figure 1**. This structure provides these smart inverters with the flexibility to operate their output voltages. By changing the amplitude and phase angle of the output voltage, the inverter can adjust its active and reactive power transmission. To illustrate the reactive power compensation mechanism of smart inverters, **Figure 2** shows two typical operation modes, which provide pure capacitive or inductive reactive power to the grid.

As shown in **Figure 2**, the reactive power compensation modes are determined by the voltage of smart inverters. The yellow circle range in **Figure 2** is drawn based on the limitation of the rated current, which protects the inverter from over-loading. As the inverter voltage varies within this yellow circle, the current changes accordingly. Then, the inverter gives out both active power P and reactive power Q according to the current and the grid voltage. The operation range of P and Q of smart inverters is thus further determined as illustrated in **Figure 1** (Kisacikoglu et al., 2013; Su et al., 2014). However, EV chargers and PVs have different operation ranges. EV chargers can operate in four quadrants, which can absorb or give out both P and Q, while PVs do not consume any active power. Therefore, the operation range can be expressed as:

$$P^2 + Q^2 \le S_{\max}^2 \tag{1}$$

$$\begin{cases} P_{\max}^{EV} \ge P^{EV} \ge P_{\min}^{EV} \\ P^{PV} = P_{output}^{PV} \end{cases} \tag{2}$$

where $S_{\max}$ is the maximum value of the inverter capacity; P^{EV} and P^{PV} are the active power of EV chargers and PVs respectively; $P_{\max}^{EV}$ and $P_{\min}^{EV}$ denote the maximum and minimum allowed active charging power for EV chargers respectively; P_{output}^{PV} is the active power generated by PVs.

Eq. 1 indicates that when chargers and PVs are idle, these smart inverters are capable of providing considerable reactive power compensation. This advantage is illustrated by the orange rectangle in **Figure 1**, where the inverter has a vast operation range under low active power level.

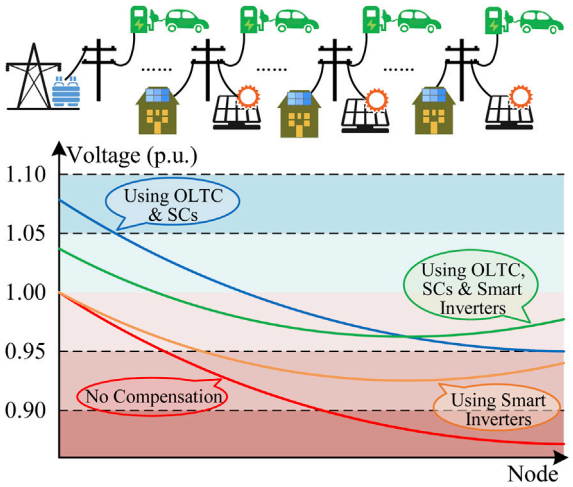

FIGURE 3 | Voltage diagrams of different compensation strategies.

2.2 Models of On-Load Tap Changers and Switching Capacitors

OLTCs and SCs are fundamental voltage regulation resources in DNs, which are usually equipped at the transformer substation. The reactive power compensation mechanism for OLTCs is to change the turn ratio by adjusting the tap position. The model of the OLTCs can be expressed as (Wu et al., 2017)

$$k_{ij} = k_{ij}^{\min} + tap_{ij} \cdot \Delta k_{ij}, 0 \le tap_{ij} \le \overline{tap_{ij}} \tag{3}$$

where k_{ij} is the turns ratio of the transformer between node i and node j; $k_{ij}^{\min}$ is the minimum turns ratio; tap_{ij} is the tap position of the OLTC; $\overline{tap_{ij}}$ is the maximum value of the tap position; Δk_{ij} is the ratio change per tap.

SCs provide capacitive reactive power to maintain the voltage level. According to the capacity of each SC connected to the grid, the model of SCs can be described as

$$Q_{SC} = \sum_{i=1}^{N_{SC}} (Q_i^{SC} \cdot n_i^{SC}), 0 \le n_i^{SC} \le \overline{n_i^{SC}} \tag{4}$$

where Q_{SC} is the total reactive power provided by SCs; N_{SC} is the total number of the SC types; Q_i^{SC} and n_i^{SC} are the capacity and the number of SCs that belong to type i; $\overline{n_i^{SC}}$ is the maximum value of n_i^{SC}.

2.3 Comparisons of Different Compensation Strategies

Since OLTCs and SCs are commonly located in the transformer substation, traditional compensation methods regulate the voltage levels by injecting reactive power at the head of the feeders, resulting in the difficulty of balancing the voltage of

the whole feeder line. **Figure 3** illustrates the effect of different compensation strategies. When the voltage violation occurs, the voltage profile with no compensation adopted drops seriously at the feeder terminal. Although the OLTC and SCs are able to raise the voltage profile as shown in the blue line, they cause over-voltage at the head of feeders because of too much reactive power injection.

Smart inverters can regulate the voltages at the demand side in a local way, as they are distributed close to terminal users in DNs. Therefore, smart inverters are capable of compensating reactive power locally as the orange line in **Figure 3** depicts. However, in severe voltage violations, smart inverters may not be able to raise all voltages above the safe line due to the limited capacities of demand-side power electronics.

The green line in **Figure 3** illustrates that by using both traditional compensation resources and smart inverters, a satisfactory compensation effect can be achieved without causing over-compensation or being constrained by capacities, which is feasible for voltage regulation in DNs.

2.4 Voltage Deviation Indexes

To further evaluate the voltage deviation, the voltage violation probability P_{vio} and the expected comprehensive deviation of voltage violations E_{dev} are proposed in this paper. The definition of voltage violations in this paper is the scenario where any nodal voltage exceeds the safe range, which is set as 0.95 p. u. to 1.05 p. u. In MCMC simulation analysis, P_{vio} can be expressed as the proportion of voltage violation scenarios in all simulated scenarios:

$$P_{vio} = \frac{1}{N_{sim}} \sum_{i=1}^{N_{sim}} L_i^{vio} \tag{5}$$

$$L_i^{vio} = \begin{cases} 1, & \text{the voltage violation happens} \\ 0, & \text{no voltage violation happens} \end{cases} \tag{6}$$

where N_{sim} is the number of all simulated scenarios and L_i^{vio} marks the simulation result in the i^{th} scenario.

E_{dev} describes the deviation degree of the voltage violation. The expression of E_{dev} is

$$E_{dev} = \frac{1}{N_{sim}} \sum_{i=1}^{N_{sim}} D_i \tag{7}$$

$$D_i = \sqrt{\frac{\sum_{j=1}^{N_{node}} \left[V_j(i) - V^{ref} \right]^2}{N_{node}}} \tag{8}$$

where D_i is the comprehensive voltage deviation of the i^{th} scenario; N_{node} is the number of nodes in the DN; $V_j(i)$ is the nodal voltage of node j in the i^{th} scenario; V^{ref} is the reference nodal voltage, which is set to 1 p. u. in this paper.

3 SIMULATION METHODS FOR VOLTAGE VIOLATION ASSESSMENT

3.1 Kernel Density Estimation of Electric Vehicle Loads and Photovoltaics Outputs

The KDE method is utilized to model the PDFs of EV loads and PV outputs. Its basic idea is to treat each sample as a kernel function and sum these functions to form an overall PDF. Several load samples and the normal distribution kernel function are selected in **Figure 4** to illustrate the mechanism of KDE.

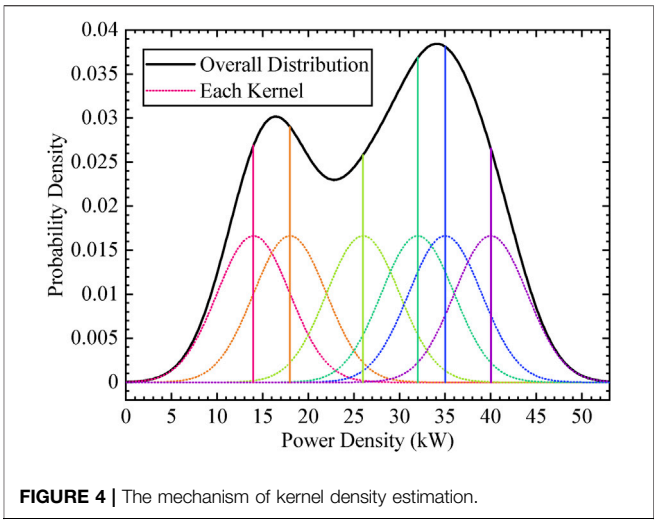

FIGURE 4 | The mechanism of kernel density estimation.

Different kernel functions create different PDFs of the sample data. With the kernel function defined as $K(\cdot)$, the PDF estimated by KDE is (Bowman and Azzalini, 1997)

$$\tilde{f}(x) = \frac{1}{N_{sam}h} \sum_{i=1}^{N_{sam}} K\left(\frac{x - X_i}{h}\right) \tag{9}$$

where N_{sam} is the number of sample data; h is the bandwidth; $X_1, X_2, \ldots, X_n$ are the sample data from the target distribution.

The standard normal distribution kernel function is adopted in this paper. Hence, **Eq. 9** can be specified as

$$\tilde{f}(x) = \frac{1}{N_{sam}h} \sum_{i=1}^{N_{sam}} \frac{1}{\sqrt{2\pi}} e^{\frac{(x-X_i)^2}{2h^2}} \tag{10}$$

To avoid over-smooth or under-smooth in KDE, the bandwidth h is determined according to the formula provided by Silverman (2018).

$$h = \left(\frac{4}{3N_{sam}}\right)^{1/5} \sigma \tag{11}$$

where σ is the standard deviation of the sample data.

3.2 Slice Sampling for Voltage Violation Assessment

It is essential to accurately sample from the PDF obtained by KDE to generate adequate data for MCMC simulation. Slice sampling is an efficient method for handling the continuous PDF with an irregular shape and is mainly composed of two procedures as illustrated in **Figure 5** (Neal, 2003).

The first procedure is defined as the step-out process in **Figure 5A**. Assume x_k is the previous sampling result and y_k is an auxiliary variable randomly drawn from $U[0, \tilde{f}(x_k)]$. The step-out process is to extend the slice range from the initial point

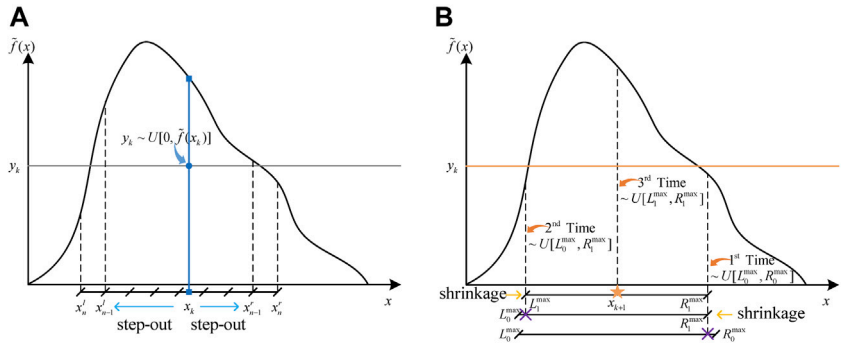

FIGURE 5 | Procedures of slice sampling **(A)** is the step-out process **(B)** is the shrinkage process.

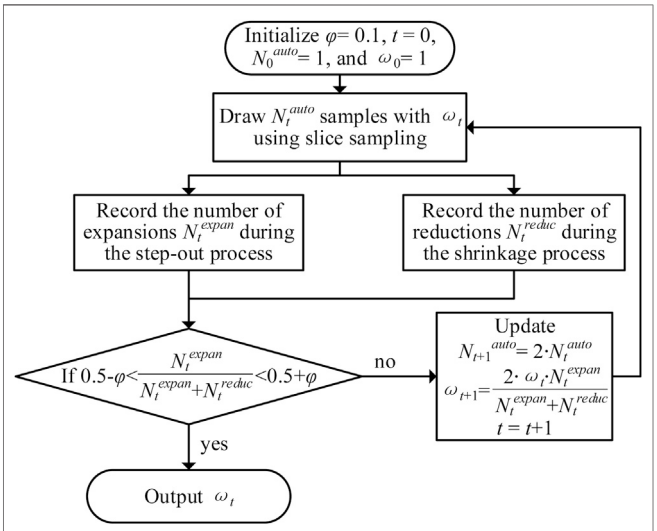

FIGURE 6 | Flow chart of the step width selection.

of x_k step by step in a step width of ω until the probability densities of both ends are all below y_k. Therefore, the eventual slice range completely contains the PDF range which is above y_k.

Then, the shrinkage process is carried out to obtain the next sample x_{k+1} that satisfies $\tilde{f}(x_{k+1}) \geq y_k$. In **Figure 5B**, $L_0^{\max}$ and $R_0^{\max}$ are the initial values of the left end and the right end of the slice range respectively. The first sample is drawn from $U[L_0^{\max}, R_0^{\max}]$ with its corresponding PDF value calculated. If the value is below y_k, the new slice range boundary will be updated and the next sample will be drawn according to the new range until the sample satisfies $\tilde{f}(x_{k+1}) \geq y_k$. The step-out and shrinkage procedures continue to provide samples until the simulation converges.

3.3 Automated Step Width Selection for Slice Sampling

The inappropriate value of the step width ω can decrease the sampling efficiency significantly. Therefore, the automated selection mechanism is introduced in this paper to find the optimal ω (Tibbits et al., 2014).

The selection algorithm is shown in **Figure 6**. This algorithm helps to minimize the effort of step-out and shrinkage operations with several pre-sampling iterations. In each iteration, the numbers of step-out and shrinkage operations are recorded to optimize ω until the tuning iteration converges. After that, the optimal ω is utilized in slice sampling to accelerate the MCMC simulation.

4 RISK ASSESSMENT FOR VOLTAGE VIOLATION

In this section, the tap position of the OLTC and the reactive power from smart inverters and SCs are regarded as manipulated variables to regulate voltage violations in DNs. As different EV loads and PV outputs are sampled from the slice sampling methods, these manipulated variables are optimized to minimize the voltage deviations in each simulation. P_{vio} and E_{dev} are also calculated during the simulation. When P_{vio} and E_{dev} converge, the MCMC simulation stops and outputs the final risk assessment results.

4.1 Voltage Regulation Models

The voltage regulation models proposed in this paper only utilize the remaining reactive power capacities of smart inverters. The total reactive power compensation provided from node i is

$$Q_i = \sum_{j=1}^{N_i^{SI}} Q_i^j \tag{12}$$

where Q_i^j is the reactive power by the j^{th} smart inverter of node i and N_i^{SI} is the number of smart inverters in node i.

Besides, the tap position and n_i^{SC} of SCs are also controlled in the voltage regulation. Their models are expressed in **Eq. 3** and **Eq. 4**. Based on the above equations, the power flow model is (Saadat, 2011)

$$\begin{cases} \Delta P_i = -P_i^{load} - V_i \sum_{j=1}^{N_{node}} V_j \left(G_{ij} \cos\theta_{ij} + B_{ij} \sin\theta_{ij} \right) = 0 \\ \Delta Q_i = Q_i - Q_i^{load} - V_i \sum_{j=1}^{N_{node}} V_j \left(G_{ij} \sin\theta_{ij} - B_{ij} \cos\theta_{ij} \right) = 0 \end{cases} \tag{13}$$

where P_i^{load} and Q_i^{load} are the active and reactive power consumed by loads in node i respectively; V_i is the nodal

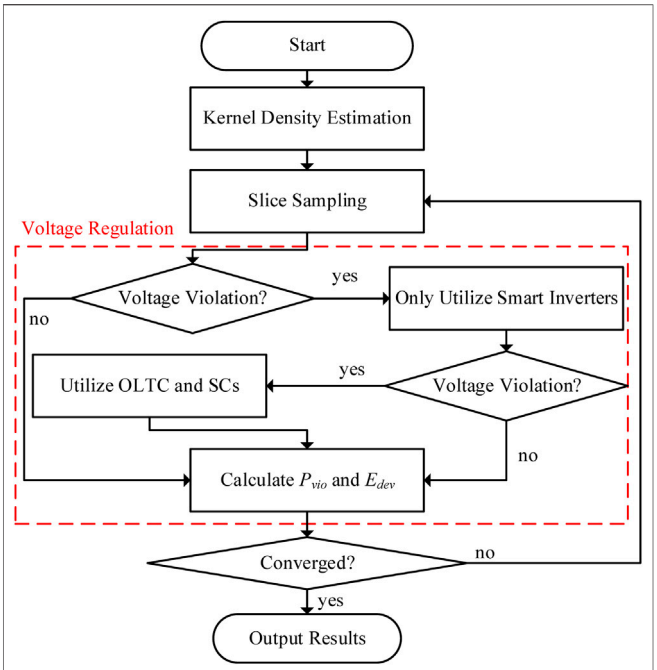

FIGURE 7 | Flow chart of the risk assessment.

voltage of node i; θ_{ij} is the voltage phase angle difference of node i and node j; G_{ij} and B_{ij} are the conductance and susceptance of the nodal admittance matrix elements in row i and column j respectively.

4.2 Voltage Regulation Constraints

Eq. 3 and **Eq. 4** show the operational constraints of the OLTC and SCs. The operation range of smart inverters is

$$-\sqrt{\left(S_i^{j,max}\right)^2-\left(P_i^j\right)^2}<Q_i^j<\sqrt{\left(S_i^{j,max}\right)^2-\left(P_i^j\right)^2} \tag{14}$$

where $\left(S_i^{j,max}\right)^2$ is the maximum capacity of the j^{th} smart inverter of node i and P_i^j is the active power from the j^{th} smart inverter of node i.

Apart from constraints of reactive power compensation resources, the voltage regulation model is also limited by voltage amplitude constraints and transmission capacity constraints:

$$\underline{V_i}<V_i<\overline{V_i} \tag{15}$$

$$\underline{S_{ij}}<S_{ij}<\overline{S_{ij}} \tag{16}$$

$$S_{ij}=P_{ij}+Q_{ij} \tag{17}$$

where $\underline{V_i}$ and $\overline{V_i}$ are the minimum and maximum allowed nodal voltages respectively; S_{ij}, P_{ij}, and Q_{ij} are the line apparent power, active power, and reactive power between node i and node j respectively; $\underline{S_{ij}}$ and $\overline{S_{ij}}$ are the minimum and maximum allowed line capacity between node i and node j respectively.

The voltage regulation aims to minimize the nodal voltage deviation of all nodes with reactive power resources, which can be expressed as

$$\min J=\sum_{i=1}^{N_{node}}\left(V_i-V^{ref}\right)^2 \tag{18}$$

4.3 Risk Assessment Process

With the models and methods mentioned above, the risk assessment process is proposed and shown in **Figure 7**. Firstly, the KDE is carried out to derive the PDFs of EV loads and PV outputs. Then, these PDFs are utilized by the slice sampling with automated width selection to produce data samples for voltage regulation. During the voltage regulation, smart inverters are considered the first choice to reduce the operation cost of OLTCs and SCs. Moreover, voltage deviation indexes are calculated to describe the performance of regulation and estimate the convergence of MCMC simulation. If the convergence requirements are not met, the slice sampling will continue to provide samples for risk assessment.

The convergence requirements are satisfied when the accuracy indexes $\sigma(F)$ of both P_{vio} and E_{dev} are below the threshold $\underline{\sigma}$ (Green et al., 2010):

$$\sigma(F)=\frac{\sqrt{\mathrm{var}(F)}}{F},F=P_{vio},E_{dev} \tag{19}$$

where $\mathrm{var}(F)$ is the variance calculation function of F.

5 CASE STUDIES

In this section, the proposed risk assessment is carried out in a modified IEEE 33-bus distribution system (Baran and Wu, 1989). Seven charging stations and 6 PVs are randomly installed along the feeder as **Figure 8** shows. Besides, the OLTC and SCs are equipped at the head of the feeder. The capacity of each smart inverter is 550 kVA and the total capacity of SCs is 5 Mvar in this case study.

5.1 Kernel Density Estimation Results

The EV loads and PV output measurements are derived from Huang et al. (2020) and UK Power Networks (2017) respectively. The data are normalized and estimated by KDE to obtain the PDFs of EV loads and PV outputs.

Figure 9 illustrates the estimation results of KDE. To examine the goodness-of-fit, the chi-square test is performed with the significant level set at 0.05 and the degree of freedom at 49 (Su et al., 2020). The test results of the EV and PV are 23.53 and 42.40 respectively, which are both below the critical value 66.34 and validate the accuracy of KDE.

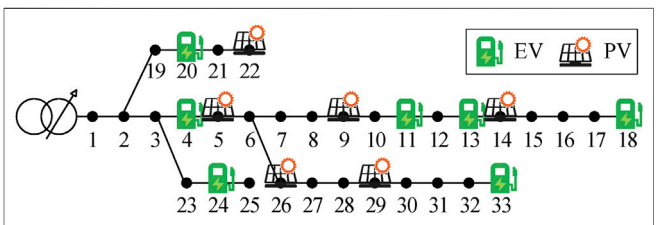

FIGURE 8 | The test feeder topology.

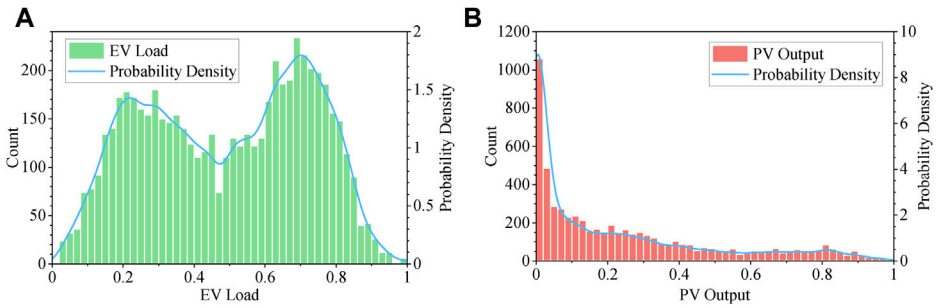

FIGURE 9 | Results of KDE **(A)** is the KDE result of EV loads with *h* as 0.02485 **(B)** is the KDE result of PV outputs with *h* as 0.02486.

TABLE 1 | Comparison of slice sampling and Monte Carlo.

Method	P_{vio}	E_{dev}	Iterations	Time (min)
Slice sampling	0.00470	0.02162	42,513	89.1
Monte Carlo	0.00465	0.02157	43,673	310.4

TABLE 2 | Voltage regulation under different cases.

Case	P_{vio}	E_{dev} (p.u.)	p_{SC}^{OLTC} (%)[a]
Only OLTC and SCs	0.96160	0.03597	100
Only smart inverters	0.17768	0.02364	0
Using above together	0.00470	0.02162	18.00

[a] p_{SC}^{OLTC} *stands for the proportion of scenarios where OLTC and SCs are utilized.*

5.2 Performance of Slice Sampling

To compare the sampling efficiency of slice sampling and the classic Monte Carlo simulation (Zhao et al., 2009), both methods are tested on an i5-4590T 2.00 GHz CPU computer through Matlab R2020a and MATPOWER 7.1 (Zimmerman et al., 2011; Zimmerman and Murillo-Sánchez, 2020). The convergence threshold is 0.01. The optimal step widths ω of EV PDF and PV PDF for slice sampling are 0.761 and 0.343 respectively. The simulation results are listed in **Table 1**.

The slice sampling only consumes 28.7% of the time of the Monte Carlo method to accomplish almost the same number of iterations and the same results of indexes. It takes more time for the classic Monte Carlo method to complete the iterations because this method rejects many unqualified samples during simulation. By contrast, no samples are discarded in slice sampling, which improves the sampling efficiency.

Table 2 illustrates three typical cases where only the OLTC and SCs, only smart inverters, and all these facilities are respectively utilized in voltage regulation. Compared with OLTC and SCs, and E_{dev} by using smart inverters decrease 81.52 and 34.28% respectively, which shows that it is more effective to compensate reactive power along the feeder *via* smart inverters. With the OLTC, SCs, and smart inverters all adopted, P_{vio} drops significantly to almost 0 and E_{dev} also gets mitigated. Besides, p_{SC}^{OLTC} in **Table 2** demonstrates that smart inverters are capable of reducing the utilization of the OLTC and SCs, which help to save the operation cost of these traditional compensation facilities.

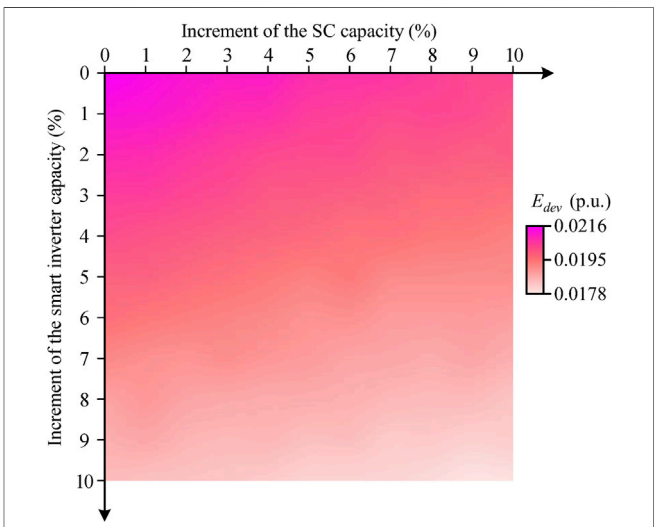

FIGURE 10 | Sensitivity analysis.

5.3 Sensitivity Analysis

In the sensitivity analysis, the capacities of smart inverters and SCs are set to increase 10% of the original value respectively. **Figure 10** depicts E_{dev} under different increments of smart inverters and SCs. P_{vio} is not illustrated since its value approximates zero and rarely varies during the simulation. If the capacity of smart inverters increases 10%, E_{dev} drops by 14.24%, while E_{dev} only drops by 5.52% if the SCs increases 10%. It can be concluded from **Figure 10** that under the same increment of capacities, smart inverters perform better in voltage regulation than SCs.

6 CONCLUSION

This paper establishes a voltage violation assessment model considering the support provided by smart inverters. With the active power samples from KDE and slice sampling, the reactive power compensation process is modeled and implemented to minimize the voltage deviation. Based on the voltage deviation indexes proposed in this paper, the case studies demonstrate that

slice sampling takes less time to converge than the Monte Carlo method. Besides, while OLTCs, SCs, and smart inverters are all essential to avoid voltage violations, smart inverters are more effective than the traditional facilities, which can save the operation cost of these facilities as well. Moreover, the sensitivity analysis shows that it is more beneficial to develop smart inverters than SCs, which validates the prospect of smart inverters for voltage regulation.

In future works, the cooperative control strategies of smart inverters for voltage regulation will be studied. The integration of both active and reactive power deliveries will be considered to further implement the four-quadrant operation characteristic of smart inverters.

DATA AVAILABILITY STATEMENT

The original contributions presented in the study are included in the article/Supplementary Material, further inquiries can be directed to the corresponding author.

AUTHOR CONTRIBUTIONS

The paper was a collaborative effort among the authors. JH designed the voltage violation assessment model. CY proposed the original idea and established the framework. WY made the case studies. WB and JW contributed to the introduction. YD contributed to the supervision and editing.

FUNDING

This work was supported in part by the National Natural Science Foundation of China under Grant 51807173, in part by the Fundamental Research Funds for the Central Universities under Grant 2021QNA4012, and in part by the Science and technology project of State Grid Zhejiang Electric Power Co., Ltd with No. 5211JX1900CV. The funders were not involved in the study design, collection, analysis, interpretation of data, the writing of this article, or the decision to submit it for publication. All authors declare no other competing interests.

REFERENCES

Abeywardana, W. D. B., Acuna, P., Hredzak, B., Aguilera, R. P., and Agelidis, V. G. (2018). Single-Phase Boost Inverter-Based Electric Vehicle Charger with Integrated Vehicle to Grid Reactive Power Compensation. *IEEE Trans. Power Electron.* 33, 3462–3471. doi:10.1109/TPEL.2017.2700944

Baran, M. E., and Wu, F. F. (1989). Network Reconfiguration in Distribution Systems for Loss Reduction and Load Balancing. *IEEE Trans. Power Deliv.* 4, 1401–1407. doi:10.1109/61.25627

Bowman, A. W., and Azzalini, A. (1997). *Applied Smoothing Techniques for Data Analysis: The Kernel Approach with S-Plus Illustrations*. Oxford and New York: Clarendon Press and Oxford University Press.

Buja, G., Bertoluzzo, M., and Fontana, C. (2017). Reactive Power Compensation Capabilities of V2G-Enabled Electric Vehicles. *IEEE Trans. Power Electron.* 32, 9447–9459. doi:10.1109/TPEL.2017.2658686

Chen, H., Prasai, A., and Divan, D. (2018). A Modular Isolated Topology for Instantaneous Reactive Power Compensation. *IEEE Trans. Power Electron.* 33, 975–986. doi:10.1109/TPEL.2017.2688393

Feng, J., Wang, H., Xu, J., Su, M., Gui, W., and Li, X. (2018). A Three-phase Grid-Connected Microinverter for AC Photovoltaic Module Applications. *IEEE Trans. Power Electron.* 33, 7721–7732. doi:10.1109/TPEL.2017.2773648

Green, R. C., Lingfeng Wang, L., and Singh, C. (2010). "State Space Pruning for Power System Reliability Evaluation Using Genetic Algorithms," in IEEE PES General Meeting, Minneapolis, MN, July 25–29, 2010 (Minneapolis: IEEE), 1–6. doi:10.1109/PES.2010.5590205

Gush, T., Kim, C.-H., Admasie, S., Kim, J.-S., and Song, J.-S. (2021). Optimal Smart Inverter Control for PV and BESS to Improve PV Hosting Capacity of Distribution Networks Using Slime Mould Algorithm. *IEEE Access* 9, 52164–52176. doi:10.1109/ACCESS.2021.3070155

Hu, B., Li, Y., Yang, H., and Wang, H. (2017). Wind Speed Model Based on Kernel Density Estimation and its Application in Reliability Assessment of Generating Systems. *J. Mod. Power Syst. Clean. Energ.* 5, 220–227. doi:10.1007/s40565-015-0172-5

Huang, S., Ye, C., Liu, S., Zhang, W., Ding, Y., Hu, R., et al. (2020). Data-driven Reliability Assessment of an Electric Vehicle Penetrated Grid Utilizing the Diffusion Estimator and Slice Sampling. *Csee Jpes*, 1–9. doi:10.17775/CSEEJPES.2020.01030

Kekatos, V., Wang, G., Conejo, A. J., and Giannakis, G. B. (2015). Stochastic Reactive Power Management in Microgrids with Renewables. *IEEE Trans. Power Syst.* 30, 3386–3395. doi:10.1109/TPWRS.2014.2369452

Kesler, M., Kisacikoglu, M. C., and Tolbert, L. M. (2014). Vehicle-to-Grid Reactive Power Operation Using Plug-In Electric Vehicle Bidirectional Offboard Charger. *IEEE Trans. Ind. Electron.* 61, 6778–6784. doi:10.1109/TIE.2014.2314065

Kisacikoglu, M. C., Ozpineci, B., and Tolbert, L. M. (2013). EV/PHEV Bidirectional Charger Assessment for V2G Reactive Power Operation. *IEEE Trans. Power Electron.* 28, 5717–5727. doi:10.1109/TPEL.2013.2251007

Neal, R. M. (2003). Slice Sampling. *Ann. Statist.* 31, 705–767. doi:10.1214/aos/1056562461

Quirós-Tortós, J., Ochoa, L. F., Alnaser, S. W., and Butler, T. (2016). Control of EV Charging Points for Thermal and Voltage Management of LV Networks. *IEEE Trans. Power Syst.* 31, 3028–3039. doi:10.1109/TPWRS.2015.2468062

Saadat, H. (2011). *Power System Analysis*. Third edn. United States: PSA Publishing LLC), 228–295.

Sharma, R., and Das, A. (2020). Extended Reactive Power Exchange with Faulty Cells in Grid-Tied Cascaded H-Bridge Converter for Solar Photovoltaic Application. *IEEE Trans. Power Electron.* 35, 5683–5691. doi:10.1109/TPEL.2019.2950336

Silverman, B. W. (2018). *Density Estimation for Statistics and Data Analysis*. Boca Raton: Routledge.

Singh, S., Pamshetti, V. B., and Singh, S. P. (2019). Time Horizon-Based Model Predictive Volt/VAR Optimization for Smart Grid Enabled CVR in the Presence of Electric Vehicle Charging Loads. *IEEE Trans. Ind. Applicat.* 55, 5502–5513. doi:10.1109/TIA.2019.2928490

Su, N., An, X., Yan, C., and Ji, S. (2020). Incremental Attribute Reduction Method Based on Chi-Square Statistics and Information Entropy. *IEEE Access* 8, 98234–98243. doi:10.1109/ACCESS.2020.2997013

Su, X., Masoum, M. A. S., and Wolfs, P. J. (2014). Optimal PV Inverter Reactive Power Control and Real Power Curtailment to Improve Performance of Unbalanced Four-Wire LV Distribution Networks. *IEEE Trans. Sustain. Energ.* 5, 967–977. doi:10.1109/TSTE.2014.2313862

Tibbits, M. M., Groendyke, C., Haran, M., and Liechty, J. C. (2014). Automated Factor Slice Sampling. *J. Comput. Graphical Stat.* 23, 543–563. doi:10.1080/10618600.2013.791193

Tómasson, E., and Söder, L. (2017). Improved Importance Sampling for Reliability Evaluation of Composite Power Systems. *IEEE Trans. Power Syst.* 32, 2426–2434. doi:10.1109/TPWRS.2016.2614831

UK Power Networks (2017). *Photovoltaic (PV) Solar Panel Energy Generation Data*. London, United Kingdom: London Datastore. Available at: https://data.london.gov.uk/dataset/photovoltaic–pv–solar-panel-energy-generation-data.

Ustun, T. S., Aoto, Y., Hashimoto, J., and Otani, K. (2020). Optimal PV-INV Capacity Ratio for Residential Smart Inverters Operating under Different Control Modes. *IEEE Access* 8, 116078–116089. doi:10.1109/ACCESS.2020.3003949

Varma, R. K., and Siavashi, E. M. (2018). PV-STATCOM: A New Smart Inverter for Voltage Control in Distribution Systems. *IEEE Trans. Sustain. Energ.* 9, 1681–1691. doi:10.1109/TSTE.2018.2808601

Wu, W., Tian, Z., and Zhang, B. (2017). An Exact Linearization Method for OLTC of Transformer in Branch Flow Model. *IEEE Trans. Power Syst.* 32, 2475–2476. doi:10.1109/TPWRS.2016.2603438

Zeraati, M., Golshan, M. E. H., and Guerrero, J. M. (2019). Voltage Quality Improvement in Low Voltage Distribution Networks Using Reactive Power Capability of Single-phase PV Inverters. *IEEE Trans. Smart Grid* 10, 5057–5065. doi:10.1109/TSG.2018.2874381

Zhao, Y., Zhang, X.-F., and Zhou, J.-Q. (2009). Load Modeling Utilizing Nonparametric and Multivariate Kernel Density Estimation in Bulk Power System Reliability Evaluation. *Proc. CSEE* 29, 27–33.

Zhou, P., Jin, R. Y., and Fan, L. W. (2016). Reliability and Economic Evaluation of Power System with Renewables: A Review. *Renew. Sustain. Energ. Rev.* 58, 537–547. doi:10.1016/j.rser.2015.12.344

Zimmerman, R. D., and Murillo-Sánchez, C. E. (2020). *MATPOWER*. Genève, Switzerland: Zenodo. doi:10.5281/zenodo.4074135 Available at: https://zenodo.org/record/4074135#.YKB4HqgzaUk (Accessed October 8, 2020).

Zimmerman, R. D., Murillo-Sánchez, C. E., and Thomas, R. J. (2011). MATPOWER: Steady-State Operations, Planning, and Analysis Tools for Power Systems Research and Education. *IEEE Trans. Power Syst.* 26, 12–19. doi:10.1109/TPWRS.2010.2051168

Conflict of Interest: The author WY was employed by State Grid Jiaxing Power Supply Company and authors WB and JW were employed by State Grid Yiwu Power Supply Company.

The remaining authors declare that the research was conducted in the absence of any commercial or financial relationships that could be construed as a potential conflict of interest.